Contract No:

This document was prepared in conjunction with work accomplished under Contract No. DE-AC09-08SR22470 with the U.S. Department of Energy.

Disclaimer:

WSRC-TR-91-138

NRTSC
NUCLEAR REACTOR TECHNOLOGY
AND SCIENTIFIC COMPUTATIONS

Keywords:
304L Stainless Steel
Pitting
Cyclic Polarization
Coupon Immersion
Impedance

Retention - Permanent

CORROSION STUDY OF REPLACEMENT MATERIALS FOR HAZARDOUS LOW LEVEL WASTE PROCESSING TANKS

by

B. J. Wiersma
Materials Technology Section

and

J. I. Mickalonis
Materials Technology Section

ISSUED: March 28, 1991

SRL SAVANNAH RIVER LABORATORY, AIKEN, SC 29808
Westinghouse Savannah River Company
Prepared for the U. S. Department of Energy under Contract DE-AC09-88SR18035

DOCUMENT: WSRC-TR-91-138

TITLE: CORROSION STUDY OF REPLACEMENT MATERIALS FOR HAZARDOUS LOW LEVEL WASTE PROCESSING TANKS (U)

APPROVALS

DATE: 4-11-91

P. E. Zapp, TECHNICAL REVIEWER
MATERIALS TECHNOLOGY

DATE: 4/11/91

J. E. Marra, MANAGER
MATERIALS TECHNOLOGY

DATE: 4/15/91

T. L. Capeletti, MANAGER
MATERIALS TECHNOLOGY

SUMMARY

New waste tanks are to be constructed in H-area to store hazardous low level wastes. AISI Type 304L (304L) stainless steel was recommended as a suitable material of construction for these tanks. Cyclic polarization and coupon tests were performed to evaluate the corrosion resistance of 304L over a wide range of waste tank environments. The results of both tests indicated that 304L was not susceptible to attack under any of these conditions. Comparison tests were also performed with ASTM A537 carbon steel (A537) and Incoloy 825. The carbon steel corroded severely in some of the environments, while Incoloy 825 did not corrode. These tests, along with those for 304L, verified the correlation between cyclic polarization and coupon tests. Electrochemical Impedance Spectroscopy (EIS) was performed to monitor the breakdown of the protective oxide film on the surface of the material as a function of time and temperature. These results also correlated with those from the cyclic polarization and coupon tests.

INTRODUCTION

Type IV tanks are available in H-area to store hazardous low level waste. The tanks receive this waste from three sources: the Sludge Processing (SP, tank #22) facility, the In-Tank Precipitation (ITP, tanks #21 and #50) process, and the Receiving Basin for Off-site Fuels (RBOF, tank #23). The sludge and precipitate will be sent to DWPF to be encapsulated in glass. The RBOF waste is routed to Tank #32 prior to being fed to the cesium removal column.

These tanks, however, do not conform to state and federal regulations for handling mixed wastes[1] which contain both radionuclides and toxins. The Type IV tanks are inadequate because they are single walled, have no secondary containment, and cannot be inspected at their outer walls. A proposal has been made to construct new tanks which meet these criteria[2]. The design of the tanks also included a more corrosion resistant material of construction. The current tanks are constructed of A285 Grade B or H212 carbon steel. The waste must be inhibited with nitrite and hydroxide to prevent corrosion[3]. 304L, which is more corrosion resistant than carbon steel, was recommended to reduce the amount of surveillance and necessary inhibitor additions during the storage of these wastes.

The composition, temperature and degree of wetness within the tanks show a wide range of variation. A review of these environmental conditions revealed that the chloride and fluoride concentrations present may induce pitting or stress corrosion

cracking of 304L[4]. Laboratory tests were conducted to evaluate the pitting resistance of 304L in the anticipated waste environments[5]. These tests included cyclic polarization, coupon test and electrochemical impedance spectroscopy (EIS). Constant extension rate tension (CERT) tests are planned to evaluate the stress corrosion cracking resistance of 304L.

EXPERIMENTAL PROCEDURE

The cyclic polarization scans were conducted according to ASTM standard G61-86. A Princeton Applied Research (PAR) Model 273A Potentiostat/Galvanostat was utilized to control the electrical potential during the test while the PAR Model 351 Corrosion Measurement System recorded the current response. The polarization scans were conducted in PAR electrochemical cells on duplicate specimens of material. The scan rate selected for these tests was 0.166 mV/s. All potentials were measured with respect to a Ag/AgCl reference electrode. The potential of this reference electrode was checked against an unused saturated calomel electrode (SCE) prior to each test.

The molar anion concentrations of the thirteen simulated waste solutions which were used for the polarization scans are summarized in Table 1[6,7]. The solution numbers which are related to the different waste types are also referenced in this table. These waste solutions, which were made from sodium salts, represent a range of concentrations which may be possible during the storage of the wastes. The initial pH of the test solutions ranged between 12 and 13.5. The expected operating temperature for the tanks is 40° C, although temperatures between 30°-60° C may be possible. Corrosion tests were performed over this range of temperatures.

Coupon tests were conducted to confirm the cyclic polarization results. Metal coupons (2" x 1" x 0.25") were partially immersed in a simulated waste environment for four months. Four coupons were hung by Teflon string in a one liter polyethylene bottle which was half filled with solution. Waterproof epoxy was applied to the sides of the coupons to prevent preferential attack of the edges. Five waste solutions, # 1, 4, 8, 11, and 13, were selected based on either a high concentration of chloride and fluoride or a lack of inhibitor species. The temperature in the bottles was controlled with a water bath for the 30° C tests and ovens for the 45° and 60° C tests. Air flow into the bottles was regulated at 100 cc/min to simulate the air flow in a waste tank. A few tests were conducted in which the air was passed through a flask which contained ascarite prior to entering the bottle. This procedure was done to remove carbon dioxide from the air so that the bulk pH could be maintained. A complete matrix of these tests is shown in Table 2. After the samples were removed, they were cleaned according to ASTM standard G1-88. Optical light and scanning electron microscopy

were used to evaluate the coupons for pit size, density and location. Energy dispersive spectroscopy (EDS) and X-ray diffraction were used to identify corrosion products or precipitated layers on the surface.

Type 304L in the solution annealed and the heat treated conditions were the primary materials of concern for both the polarization and coupon tests. The heat treatment was performed to simulate weld heat affected zones. The maximum degree of sensitization, as determined by electrochemical potentiokinetic reactivation (EPR), was obtained after heat treating the sample at 650° C for six hours. Welded coupons of 304L were also tested during the coupon tests. As a comparison, tests were also performed on A537 carbon steel and Incoloy 825 to aid in the interpretation of the results from the 304L tests. A537, which is similar to the carbon steel material used for the present waste tanks, has a lower corrosion resistance than 304L. The Incoloy 825, a nickel based alloy, is more resistant to halide attack and has a greater corrosion resistance than 304L.

EIS spectra were measured on a system that was controlled by an IBM PS/2 Model 30 personal computer with PAR Model 378 Electrochemical Impedance software. The sinusoidal waveform was generated by a PAR Model 5301A Lock-in Amplifier and applied to the sample through a PAR Model 273 Potentiostat/Galvanostat. The applied waveform had a 5 mV amplitude and a frequency range from 1 mHz to 100 kHz. The equilibrium state of the sample was characterized by measuring E_{corr} before and after each EIS test. The initial test was run after the sample was exposed for 2-3 days. The final test was performed after a three month exposure, which was just prior to removal of the sample from the test.

Samples were prepared and exposed following the procedure described above for the other samples in the coupon test except that only 2 samples were placed in each bottle. An insulated, small-diameter, copper wire was spot welded to the top of the EIS samples as a necessary electrical connection. The weld region was also covered with epoxy to prevent corrosion. The samples included solution-annealed 304L and as-received A537. The waste environments were solution #5 at 30°, 45° and 60° C. At the conclusion of the test, a visual assessment of the corrosion was made for each sample. To perform an EIS test, a reference electrode and two graphite counter electrodes were inserted through the top of the bottle. The reference electrode was a SCE placed inside a salt bridge containing a saturated potassium chloride solution. The bottles were placed in a beaker of water heated to the appropriate temperature.

RESULTS AND DISCUSSION

Cyclic Polarization Tests

Cyclic polarization provides a quick assessment of a material's pitting susceptibility. Figure 1 is an example of a polarization curve which indicates characteristic potentials and currents for assessing corrosion. The potential passes through the corrosion potential (E_{corr}) near the beginning of the scan. E_{corr} is the potential of a material in a particular solution when no external potential is applied. The current density, I_{corr}, at this potential may be determined by extrapolating the linear portions of the polarization curve until they intersect at E_{corr}. I_{corr} is related to the corrosion rate and indicates the corrosivity of an environment. As the forward scan continues, the current density increases until a maximum (I_c) is reached at the critical potential (E_c). The current then declines dramatically due to the formation of an oxide film on the metal surface (i.e., passivation). A potential region in which the metal remains passive then follows. The current density in this region is referred to as the passive current density (I_p). High values for I_c and I_p suggest that the environment is corrosive. Pitting susceptibility is indicated by the hysterisis loop which occurs between the pitting potential (E_p) and the pit protection potential (E_{pp}). At potentials greater than E_p, the protective oxide film on the metal surface breaks down locally and pits nucleate. During the initial portion of the return scan, pits continue to nucleate and propagate which results in a higher current density than observed for the forward scan. Below E_{pp}, pit growth is discontinued and no new pits are initiated.

The polarization tests indicated that A537 carbon steel was susceptible to attack in several of the waste environments. The polarization curve shown in Figure 2 is from a test performed in solution #8 at 60° C. In addition to the significant hysterisis loop, severe crevice and uniform corrosion occurred on the specimen. The greatest overall attack occurred in the dilute wash waters for ITP and SP, the 30 % variation in the average RBOF/RR concentration, and the cask decontamination cleaning solution. In each case, the waste was probably not sufficiently inhibited with nitrite or hydroxide to prevent attack by the nitrate. The amount of attack was also found to increase with temperature.

In contrast, 304L demonstrated no pitting susceptibility regardless of temperature, heat treatment or waste composition. Figure 3 shows the polarization curve for the test performed on solution annealed 304L in solution #1 at 60° C. This curve is

representative of all the tests that were conducted. No characteristic hysterisis loop or attack of the specimen surface was observed. The sharp peaks observed on the return scan may be due to either repassivation, deposition, or surface reactions.

The Incoloy 825 specimens were also not susceptible to pitting in any of the waste environments. Figure 4 is the polarization curve for the test performed in solution #1 at 60° C. Again, no hysterisis loop or specimen attack was observed for any of the waste solutions.

I_C and I_P were measured to determine the relative corrosivity of the waste environments for a given material. Additionally, these parameters may help determine which material is more corrosion resistant in the wastes. Figures 5-8 show I_C and I_P for 304L and Incoloy 825 (A 537 did not exhibit these values). In general, the values of I_C and I_P were the same magnitude for the two materials and were found to increase with temperature. For solutions #1, 3, 4, and 6 the values Ic and Ip were lower for Incoloy 825 than 304L. This result may be due to the greater corrosion resistance of Incoloy 825 to the higher chloride and fluoride concentrations in these wastes. These concentrations, however, did not result in significant attack of either material.

Coupon Tests

The results of the coupon tests for all materials showed good agreement with their results from the cyclic polarization scans. As expected, corrosion was not observed on either the 304L or Incoloy 825 coupons in any of the solutions tested. Incoloy 825 and A537, however, were tested in solutions #1 and 8 only. The cyclic polarization scans predicted that A537 would not be attacked in solution #1, while those in solution #8 would corrode severely. The coupons which were immersed in solution #1 were not corroded. The coupons which had been in solution #8, however, were covered with isolated patches of rust in the section of the coupon which was not immersed, i.e., the vapor area, at the water line and in the crevice beneath the epoxy. The quantity of surface area covered by rust increased with solution temperature. After cleaning the sample, the area beneath the rust was examined and found to exhibit a shallow crater-like appearance. The immersed area of the coupon did not exhibit corrosive attack.

The results from the A537 coupon tests correlated well with observations of the present tank walls[8]. For example, Tank #23 contained an uninhibited RBOF waste similar to solution #8. Upon cleaning this tank, shallow crater-like attack was seen at the water line and in the vapor area, while the immersed area did not corrode. The attack observed in the vapor and waterline areas may have occurred beneath deposits which were present in

these areas. Tanks #21, 22, and 50 stored inhibited waste solutions similar to solution #1. Precipitates formed on the wall in the vapor area and the cooling coils in these tanks, but corrosion was not observed. Corrosion may be controlled then by either proper inhibition of the waste solution or selection of a material such as 304L.

As indicated above, precipitate layers were observed on the coupons which had been immersed in solutions #1, 4, 8, and 13. The morphology and compositon of the precipitate layers appear to depend on the temperature and composition of the waste solution, but not on the material. Except for case of vapor areas of A537 coupons in solution #8, there was no indication of corrosion occurring beneath these precipitates on any of the coupons.

A complete description of the precipitates is given in Table 3. The vapor areas of the coupons which were immersed in solutions #1, 4, 8, and 13 were covered with isolated patches of white, coalesced cubic crystals composed primarily of aluminum. The density of the patches, which were identified as gibbsite (α-$Al_2O_3 \cdot 3H_2O$), increased with temperature and concentration of the aluminate anion ($Al(OH)_4^-$) in the solution. The aluminate anion appears to be involved in the precipitation process since solution #11, which does not contain this anion, did not deposit any of these crystals.

The morphology and composition of the immersed area precipitates were more dependent on the solution composition than those in the vapor area. For example, precipitates on coupons that had been immersed in solution #1 were small 3-4 μm size beads which contained aluminum, silicon and sodium. As the temperature increased, the size and density of the beads decreased and the surface of the coupon became darker. The beads also appeared in the area beneath the epoxy adjacent to the immersed area, although they were less dense in this area. In contrast, the precipitates from solution #8 appeared as cracked, mud-like flakes which gave the surface a multicolored luminescent luster. At 30° C these flakes were composed of aluminum, phosphorous and sodium, while at 60° C they contained silicon rather than phosphorous. The area beneath the epoxy contained a small amount of these precipitates which indicates that the epoxy did not completely prevent exposure to the waste solution.

EIS Tests

EIS is an AC electrochemical technique for analyzing the time and frequency dependence of a corrosion process. A small-amplitude sinusoidal voltage waveform is applied to the sample and the current and potential responses are monitored. The responses are measured over a range of frequencies. This technique causes only a small disruption of the test sample from

its equilibrium or rest state, i.e. at E_{corr}. The impedance, which is the voltage divided by the current, is determined at each frequency to develop the impedance spectrum. One way that spectra are displayed is as Bode plots, which are the absolute magnitude of the impedance, |Z|, and the phase angle plotted as a function of the frequency. The Bode plots are analyzed in terms of electrical components, such as resistors and capacitors, which are correlated to the electrochemical state and corrosion process of the test material. The impedance spectra can reveal the onset of corrosion when measured over time.

In this study, EIS was combined with the coupon test for a small number of samples to monitor for corrosion. Initially, the onset of pitting or general corrosion was to be detected. Equipment and laboratory problems, however, limited the results to an initial and final measurement which demonstrated the correlation of EIS test results to those for both the coupon test and cyclic polarization.

EIS test results correlated well with the visual assessment of both the 304L and A537 samples. The EIS test results are summarized in Figures 9-14 as Bode plots of |Z| and the phase angle. The figures show the actual results for one of the samples at each temperature. Figures 9 and 10 are plots of |Z| and the phase angle for A537 at the start of the coupon test, respectively. Figures 11 and 12 are plots of |Z| and the phase angle for A537 at the finish of the coupon test, respectively. The final Bode plots of |Z| and the phase angle for 304L are shown in Figures 13 and 14, respectively.

Since the initial results for 304L and A537 were similar in shape only those for A537 are presented. The results showed that after a short exposure both materials displayed primarily a capacitive behavior which was independent of temperature. This behavior occurs for materials with either a passive oxide or surface layer. The capacitive behavior was characterized in the low frequency range (10 mHz-10 Hz) by the linear, negatively-sloped line shown in Figure 9 and by the phase angle approaching 90 degrees shown in Figure 10. The high frequency range (>100 Hz) is dominated by the solution resistance which is seen as a frequency-independent |Z| value in Figure 9 and by the phase angle approaching 0 degrees in Figure 10. The solution resistance was the same for both 304L and A537.

Although the impedance spectra for 304L and A537 were similar in shape, |Z| values for 304L were greater than those for A537 by an order of magnitude at frequencies less than 100 Hz. This greater impedance signified that 304L was more corrosion resistant than A537. At frequencies less than 10 mHz, some A537 samples showed that |Z| leveled off with a corresponding decrease in the phase angle. These changes, however, may indicate localized weakening of the passive oxide layer on A537.

The final EIS spectra as shown in Figures 13 and 14 for 304L were nearly identical to the initial spectra. The results were again independent of temperature. The lack of any change indicated that 304L maintained its passive oxide layer without any localized or general corrosion. If corrosion occurred on these samples, then changes in the low frequency range (<10 Hz) would have been observed. E_{corr} for the samples changed over the course of the coupon test. Initial E_{corr} values ranged from -0.050 to +0.005 V (SCE) and final values ranged from +0.070 to +0.140 V (SCE). A temperature dependence of E_{corr} was not apparent.

Visual inspection of the samples found no obvious corrosion, although a deposited surface layer was found on immersed sections of the samples. Such a layer may influence the EIS spectra. A more rigorous deconvolution analysis of the results will be attempted to determine any possible changes in the spectra. The EIS spectra, however, clearly showed that the samples were not corroding as was observed visually. The ennoblement of E_{corr}, however, may be due to the formation of this surface layer. The surface layer had a fine granular structure at all temperatures and appeared the thickest on the samples exposed at 45° C. Small deposits were sporadically located on the part of the sample not immersed.

The final EIS spectra for A537 were significantly different from the initial spectra as shown by a comparison of Figures 9-12. The shape of the spectra changed and the results had a temperature dependency. Figures 11 and 12, which show the final Bode plots, were indicative of a corroding material. In the low frequency range (<10 Hz), final |Z| values were approximately an order of magnitude lower than the initial values and decreased with increasing temperature. A lower impedance is indicative of a less corrosion resistant material. The decrease in |Z| corresponded with a decrease in the maximum value of the phase angle and a shift in the maximum to higher frequencies. The shift results from the presence of a corrosion process which is a low frequency phenomenon. The change in the EIS spectra was accompanied by a change in E_{corr}. Initial values ranged from -0.025 to -0.20 V (SCE) and final values ranged from -0.180 to -0.240 V (SCE). A temperature dependence was not observed.

The visual assessment of the A537 samples revealed that corrosion was occurring. The sections of the coupons not immersed were the most corroded as was seen for the other waste solutions. The corrosion products had a tubular and flake morphology. The size of the corroded area decreased with decreasing temperature. The immersed sections had a surface layer similar to that observed for 304L. The layers on the samples exposed at 45° C were once again thicker. The samples at all temperatures had some corroded spots on the immersed sections. Extensive corrosion was also observed beneath the epoxy. The results of the visual inspection correlated with the

those of the EIS test; both results showed corrosion was occurring. The shift in E_{corr} to more active values was a result of this corrosion.

The visual assessments of the EIS coupon samples were similar to those for the coupons exposed to solution #8, which is the ± 30% variation of the average composition of the RBOF/RR waste. The presence of corrosion spots on immersed sections was not observed for this solution, which may be due to the concentration differences of these solutions. The similarity of these findings, however, clearly indicates the good correlation of results from cyclic polarization, EIS and the coupon tests.

CONCLUSIONS

The laboratory tests indicated that 304L was more resistant to corrosion in the waste environments than A537 and is a suitable material of construction for the hazardous low level waste tanks. Good agreement between the results from the polarization scans and the coupon tests was also achieved. This agreement allows for confidence to be placed in the cyclic polarization technique as a quick and efficient means of determining corrosion resistance in the waste environments. The EIS results were also in agreement with those from the coupon tests. Thus, the EIS technique was demonstrated to be an effective means for monitoring corrosion processes as a function of temperature and time.

Future Corrosion Testing

Further coupon tests are being conducted on A537 and Incoloy 825 for comparison with 304L and to verify the correlation with the cyclic polarization and EIS tests. Coupon tests are also being performed to investigate the effect of the bulk pH on precipitate formation. CERT tests will also be performed to evaluate the susceptibility of 304L to stress corrosion cracking. These tests are planned to begin in April 1991.

REFERENCES

1. J. J. Amobi to D. E. Gordon, *"Environmental Evaluation Impact Analysis Hazardous Low Level Waste Processing Tanks"*,DPSP-88-1049, May 3, 1988.

2. G. M. Johnson to D. M. Bove, *"Savannah River Plant - Waste Management Projects Hazardous Low Level Waste Processing Tanks (FY 1990 Line Item) CAB Basic Data - Revision 1"*, WCC- 87-363, September 18, 1987.

3. DPST-241-3.01, 5.01, 5.02, and 5.03.

4. R. S. Ondrejcin to J. E. Black, *"Corrosion Program for Hazardous Low Level Waste Tanks"*, DPST-88-663, June 24, 1988.

5. J. I. Mickalonis to D.T. Hobbs, *"Corrosion Study of Replacement Materials for Hazardous Low Level Waste Processing Tanks"*,WSRC-TR-90-74-1, January 31, 1990.

6. D. T. Hobbs, *"Corrosion Test Program for Hazardous Low Level Waste Processing Tanks"*, WSRC-RP-89-17, April 5, 1989.

7. P. D. d'Entremont to D. T. Hobbs, *"Composition of Waste solutions in the HLLWPT"*, July 12, 1988.

8. Private communication with F. G. McNatt, March 6, 1991.

Table 1. MOLAR ANION COMPOSITIONS OF LOW LEVEL HAZARDOUS WASTE

-SP and ITP Wash Waters
-RBOF/Resin Regeneration

WASTE SOLUTIONS

SOLUTION NUMBER	1	2	3	4	5	6	7	8
pH	13.7	12.0	13.5	13.5	12.0	13.1	12.9	12.7
OH^-	2.1	0.03	1.1	1.3	0.024	0.66	0.21	0.15
$CO_3^=$	0.1	0.0015	0.051	0.16	0.0023	0.081	0.14	0.098
NO_2^-	1.1	0.016	0.56	0.6	0.0085	0.3	0.1	0.07
NO_3^-	1.4	0.02	0.71	2.0	0.028	1.0	0.54	0.7
Cl^-	0.022	0.00031	0.01	0.022	0.0004	0.011	0.001	0.0013
F^-	0.011	0.00016	0.0056	0.015	0.00022	0.0076	-	-
$SO_4^=$	0.095	0.0014	0.048	0.14	0.002	0.071	0.0061	0.0079
$Al(OH)_4^-$	0.3	0.0043	0.15	0.31	0.0045	0.16	0.01	0.007
$C_2O_4^=$	0.0051	0.000073	0.0026	0.014	0.0029	0.0085	-	-
$CrO_4^=$	0.0021	0.00003	0.0011	0.0033	0.000047	0.0017	0.0012	0.00084
$MoO_4^=$	0.00027	0.000004	0.00014	0.00043	0.000006	0.00022	-	-
$SiO_3^=$	0.0021	0.00003	0.0011	0.0038	0.000054	0.0019	0.00083	0.00058
PO_4^{-3}	0.0058	0.000084	0.0029	0.0085	0.00012	0.0043	0.02	0.014

1. Decanted solution from unwashed sludge slurry
2. Final SP wash water decanted from sludge slurry
3. 1:1 mixture of 1 and 2
4. Decontaminate supernate from salt slurry
5. Final ITP wash water decanted from salt slurry
6. 1:1 mixture of 4 and 5
7. Average compositions of RBOF/resin regeneration waste
8. 30 % variation of 7 for aggressive and passivating ions

Table 1. MOLAR ANION COMPOSITIONS OF LOW LEVEL HAZARDOUS WASTE
(Continued)

-Resin Regeneration
-Tritium Target Cleaning
-Cask Decontamination

WASTE SOLUTIONS

SOLUTION NUMBER	9	10	11	12	13
pH	13.1	12.3	12.4	12.7	12.5
OH^-	0.361	0.01	-	0.01	-
NO_3^-	0.316	-	-	4.6	4.6
F^-	-	-	-	0.039	0.039
$Al(OH)_4^-$	-	-	-	0.26	0.26
$CrO_4^=$	-	0.013	0.013	-	-
PO_4^{-3}	-	0.22	0.22	-	-

9. Resin regeneration waste
10. Tritium target cleaning waste
11. Uninhibited tritium target cleaning waste
12. Cask decontamination waste
13. Unihibited cask decontamination waste

Table 2. TEST MATRIX FOR THE COUPON TESTS

SOLUTION	1	4	5	8	11	13
METAL						
304L solution annealed	x	x		x	x	x
304L heat treated	x	x		x	x	x
304L welded	x	x		x	x	x
A 537 carbon steel	x			x		
Incoloy 825	x			x		
304L solution annealed (ascarite)	xx					
304L heat treated (ascarite)	xx					
A 537 carbon steel (ascarite)	xx					
304L solution annealed impedancee			xxx			
A 537 carbon steel impedance			xxx			

x – Tests performed at 30°, 45°, and 60° C

xx – Tests performed at 45° and 60° C

xxx – Tests performed at 30°, 45°, and 60° C; two coupons per bottle.

Table 3. DESCRIPTION OF THE PRECIPITATES WHICH APPEAR ON THE COUPONS

SOLUTION	T (C)	MORPHOLOGY	THICKNESS	COLOR	CHEMISTRY
	30	**V**-White, coalesced, cubic crystals **I**-3-4 μm size beads; beads are separted so base metal can be observed	Grinding marks are not obscured	**V**-White **I**-White **E**-none	**V**-gibbsite **I**-sodium, aluminum, silicon
1	45	**V**-Larger density of crystal deposits **I**-Beads approximately the same size; density has increased	Grinding marks are not obscured	**V**-White **I**-White **E**-none	**V**-gibbsite **I**-sodium, aluminum, silicon
	60	**V**-Largest density of crystal deposits **I**-In addition to 3-4 μm size beads a large density of 1-2 μm size beads present	Grinding marks are not obscured	**V**-white **I**-black **E**-black	**V**-gibbsite **I**-sodium, aluminum, silicon
	30	**V**-White, coalesced cubic crystals **I**-3-4 μm size beads which are coalesced	Grinding marks are not obscured	**V**-White **I**-White **E**-none	**V**-gibbsite **I**-sodium, aluminum, silicon
4	45	**V**-White, coalesced cubic crystals **I**-3-4 μm size beads which are coalesced	Grinding marks are not obscured	**V**-White **I**-White **E**-none	**V**-gibbsite **I**-sodium, aluminum, silicon
	60	**V**-White, coalesced cubic crystals **I**-3-4 μm size beads which are coalesced	Grinding marks are not obscured	**V**-White **I**-White **E**-black	**V**-gibbsite **I**-sodium, aluminum, silicon
	30	**V**-White crystals are not as dense **I**-Dry, cracked flakes that are approx. 10 μm across; they are separated by 2 μm	Grinding marks are not obscured	**V**-White **I**-Green, purple **E**-Green, purple	**V**-gibbsite **I**-sodium, aluminum, phosphorous
8	45	**V**-White crystals are not as dense **I**-Two layers of flakes; top layer same as 30 C; bottom layer flakes are approx, 5 μm across and are not separated	Grinding marks are not obscured	**V**-White **I**-Green, purple **E**-Green purple	**V**-gibbsite **I**-sodium, aluminum, phosphorous, silicon

V – Vapor Area I – Immersed Area E – Epoxy Area

Table 3. DESCRIPTION OF THE PRECIPITATES WHICH APPEAR ON THE COUPONS
(Continued)

V – Vapor Area I – Immersed Area E – Epoxy Area

	60	**V**-White crystals are not as dense **I**-Layer of flakes same as at 45 C	Grinding marks are not obscured	**V**-White **I**-Blue, yellow **E**-Blue, yellow	**V**-gibbsite **I**-sodium, aluminum, silicon
	30	**V**-White, coalesced cubic crystals **I**-White, coalesced cubic crystals; octahedral crystals are embedded in the cubic crystals	Grinding marks in the immersed area are covered by 1 mm thick film which is thickest near the waterline	**V**-White **I**-White **E**-None	**V**-gibbsite **I**-sodium, aluminum, fluoride
13	45	**V**-White, coalesced, cubic crystals **I**-White, coalesced, cubic crystals	Grinding marks in the immersed area are covered by a 1 mm thick film which is thickest near the waterline	**V**-White **I**-White **E**-None	**V**-gibbsite **I**-sodium, aluminum, silicon
	60	**V**-White, coalesced, cubic crystals **I**-White coalesced, cubic crystals	Grinding marks in the immersed area are covered by a 1 mm thick film which is thickest near the waterline	**V**-White **I**-White **E**-None	**V**-gibbsite **I**-sodium, aluminum, silicon

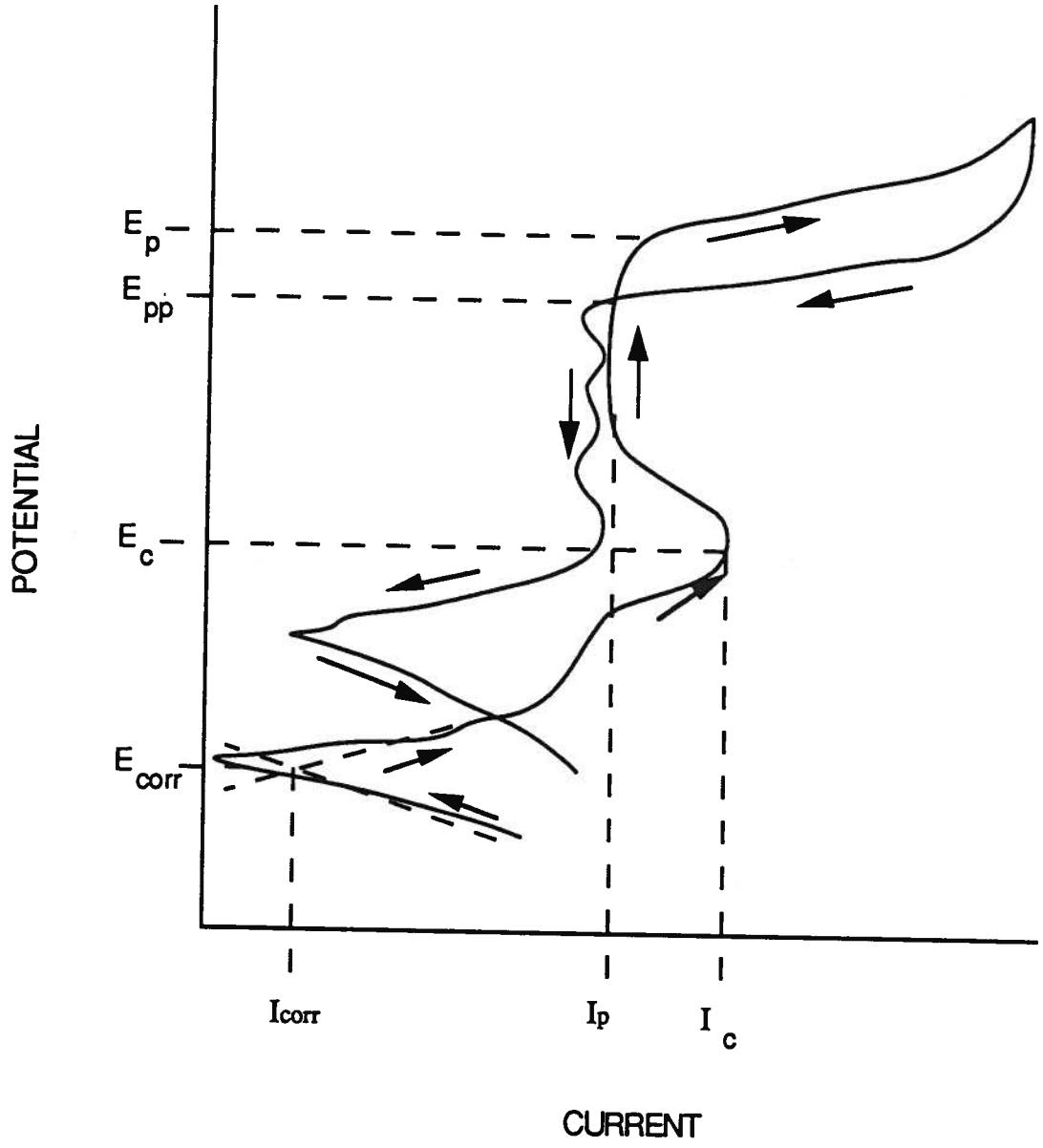

Figure 1. Typical curve generated from a cyclic polarization test.

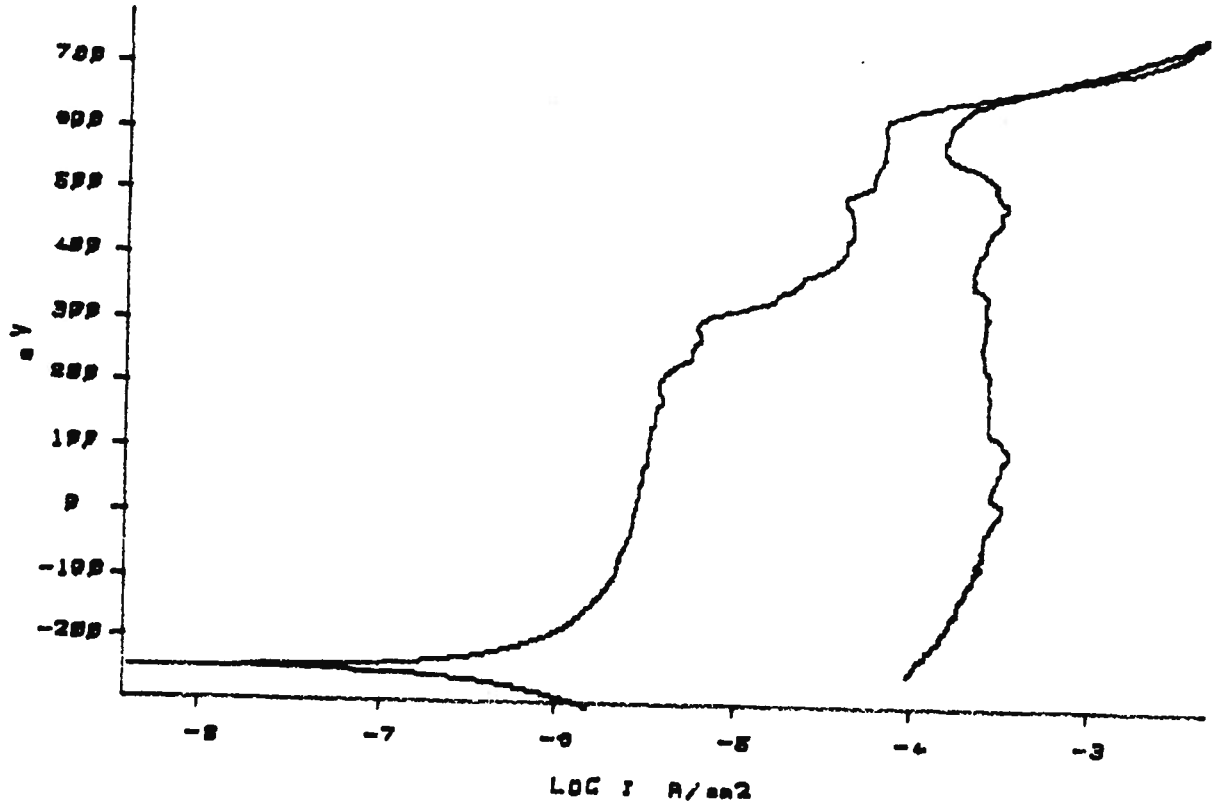

Figure 2. Polarization scan of A 537 carbon steel in waste solution # 8 at 60° C.

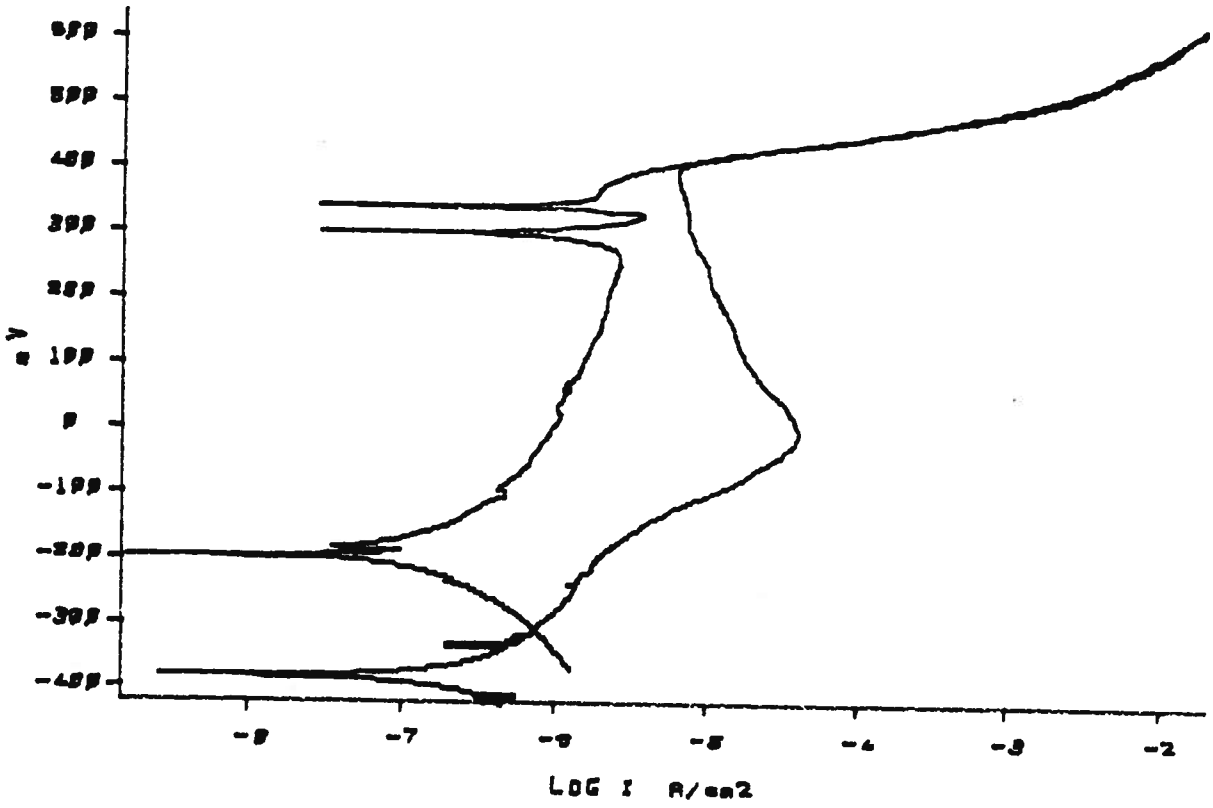

Figure 3. Polarization scan of 304L stainless steel in waste solution #1 at 60° C.

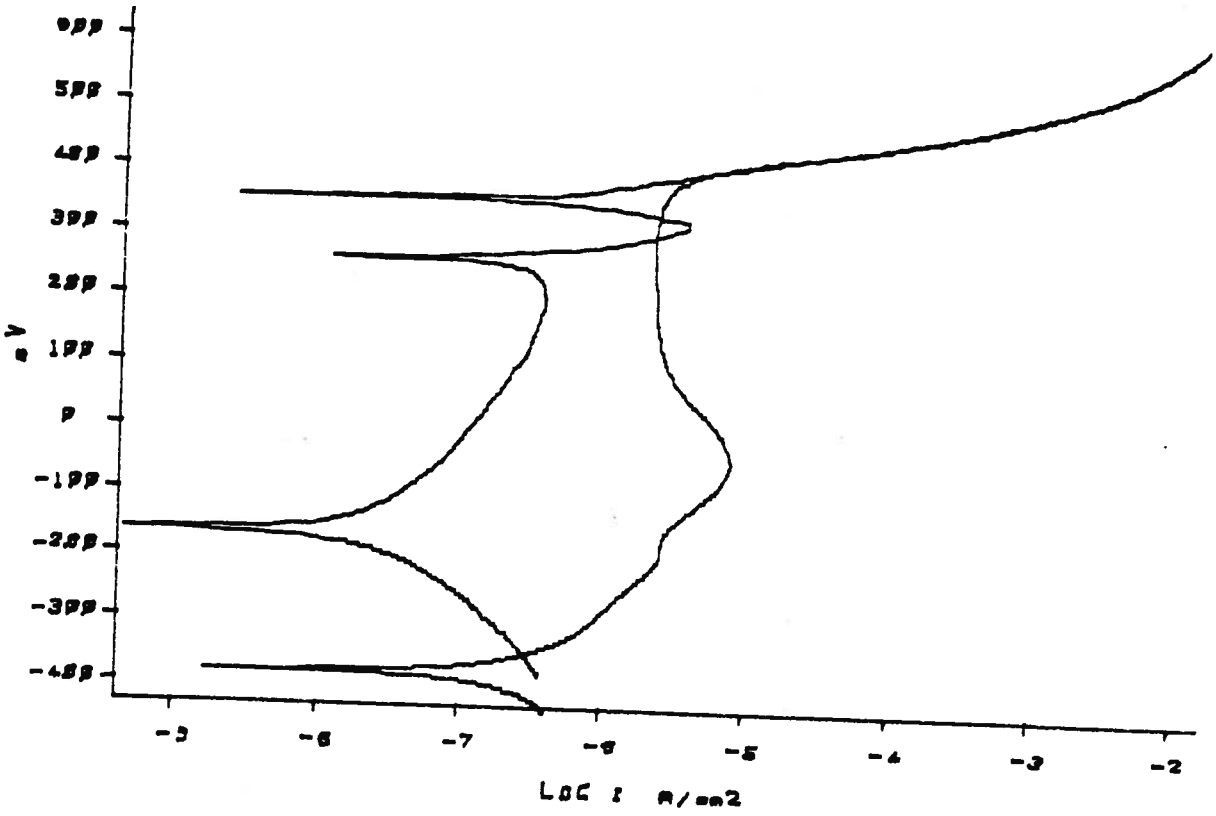

Figure 4. Polarization scan of Incoloy 825 in waste solution #1 at 60° C.

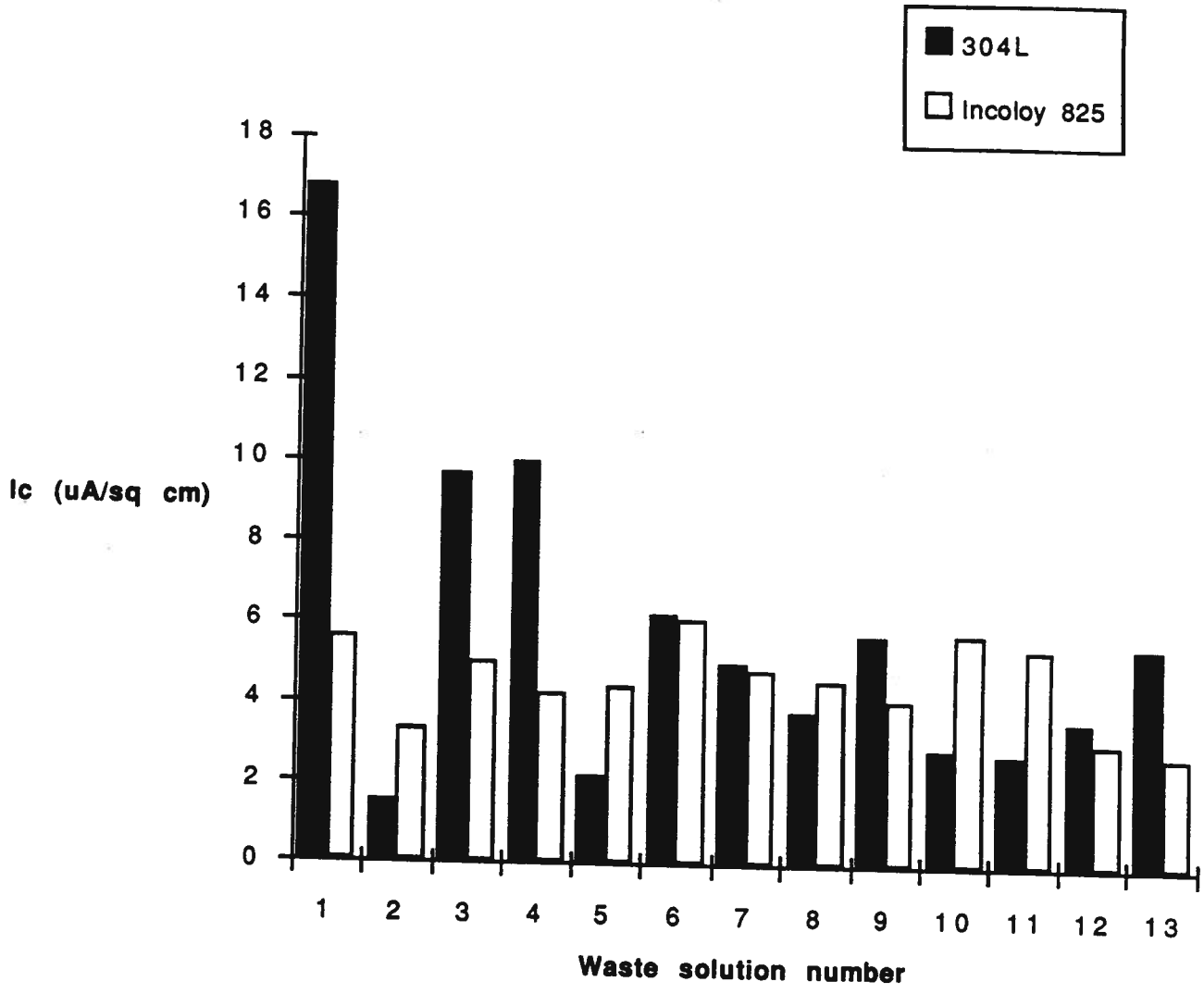

Figure 5. I_c **for the waste solutions at 30° C.**

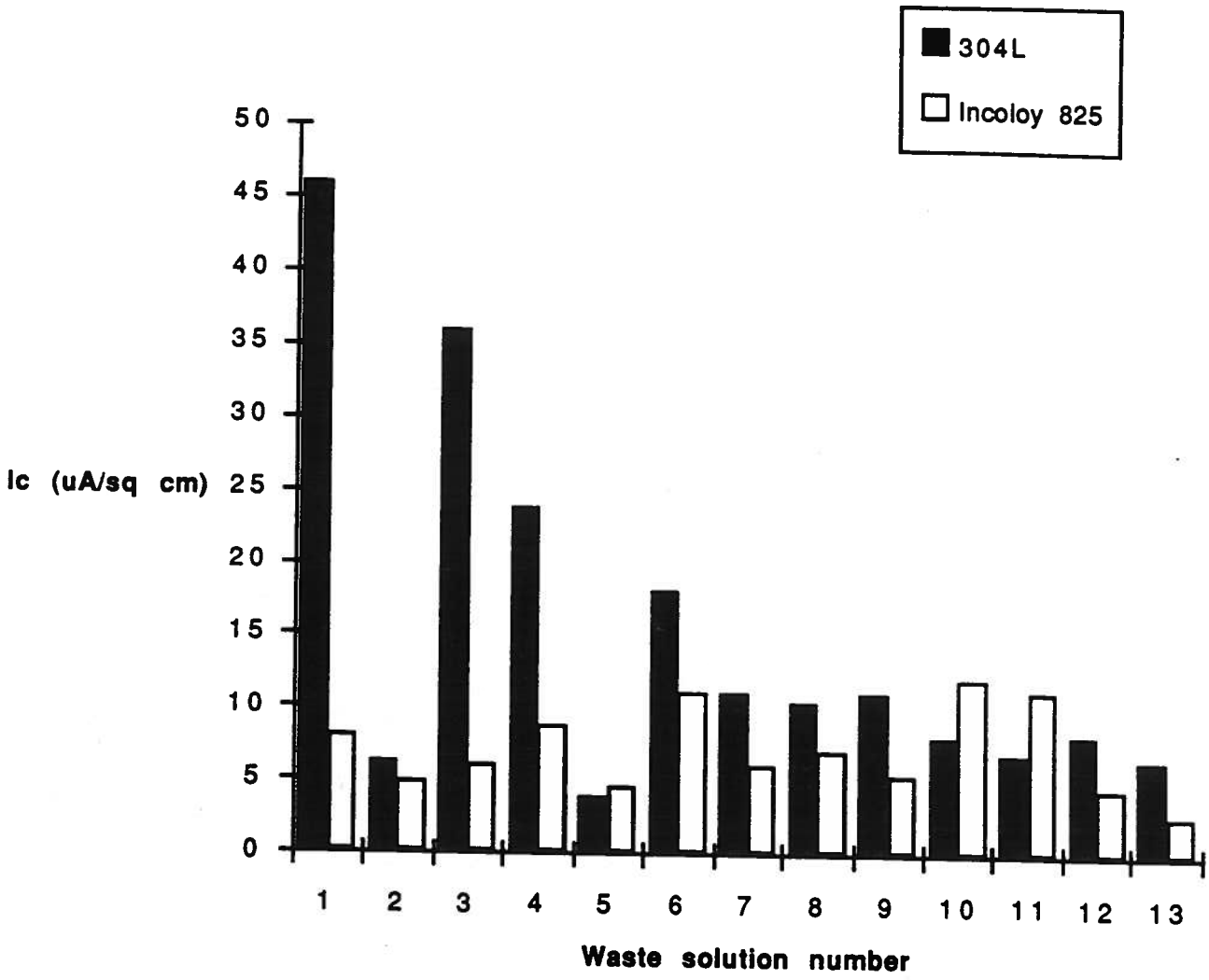

Figure 6. I_c **for the waste solutions at 60° C.**

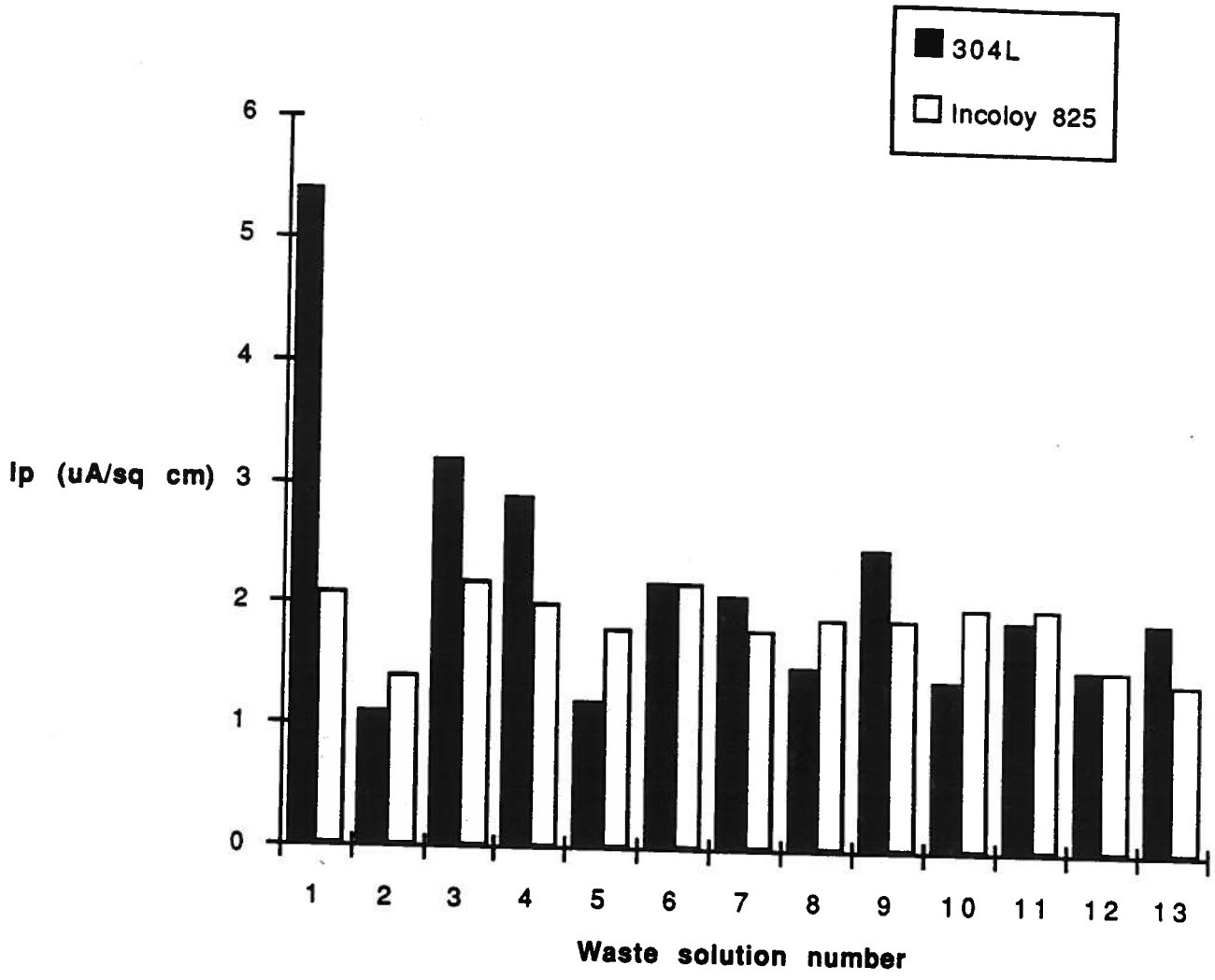

Figure 7. I_p for the waste solutions at 30° C.

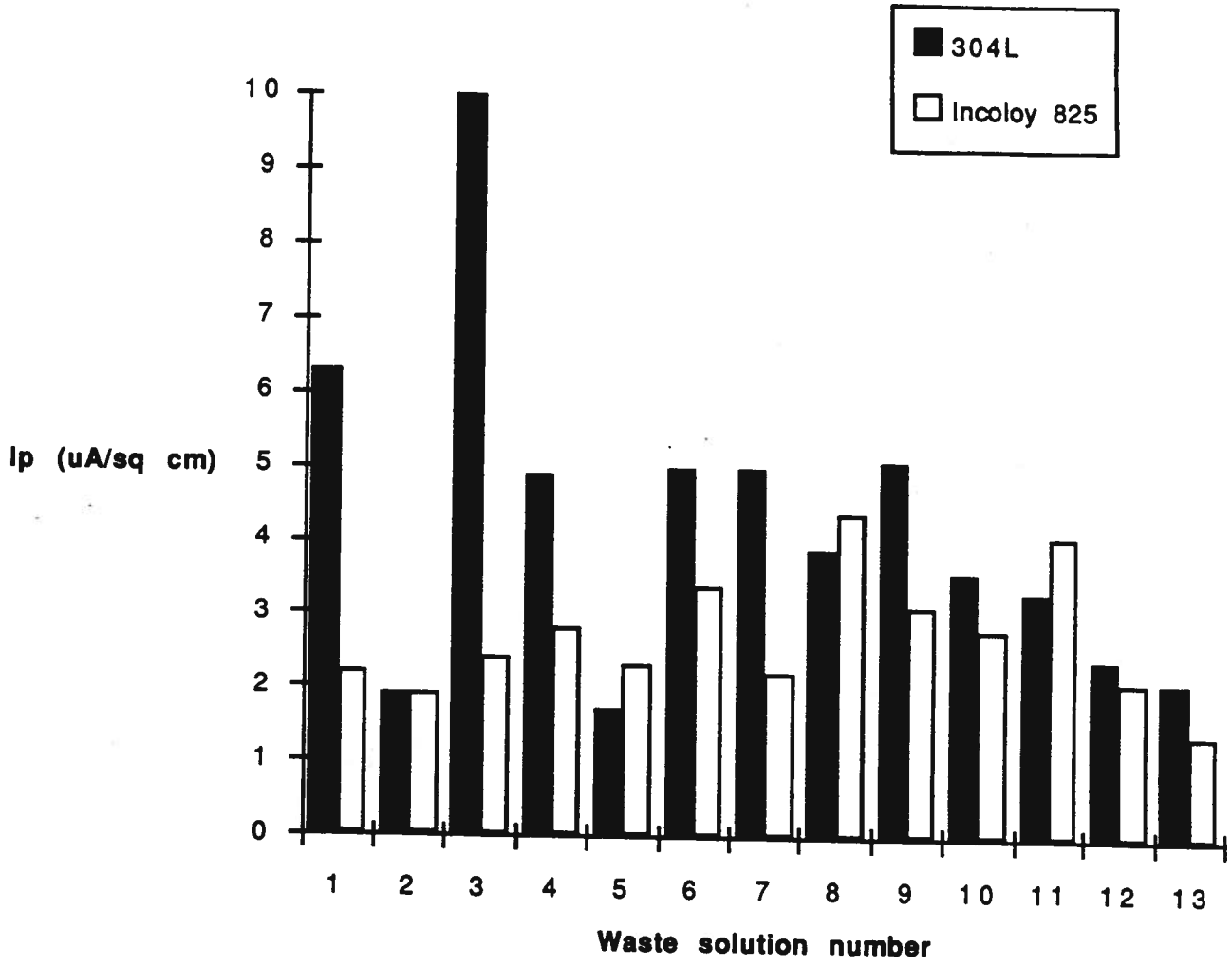

Figure 8. I_p for the waste solutions at 60° C.

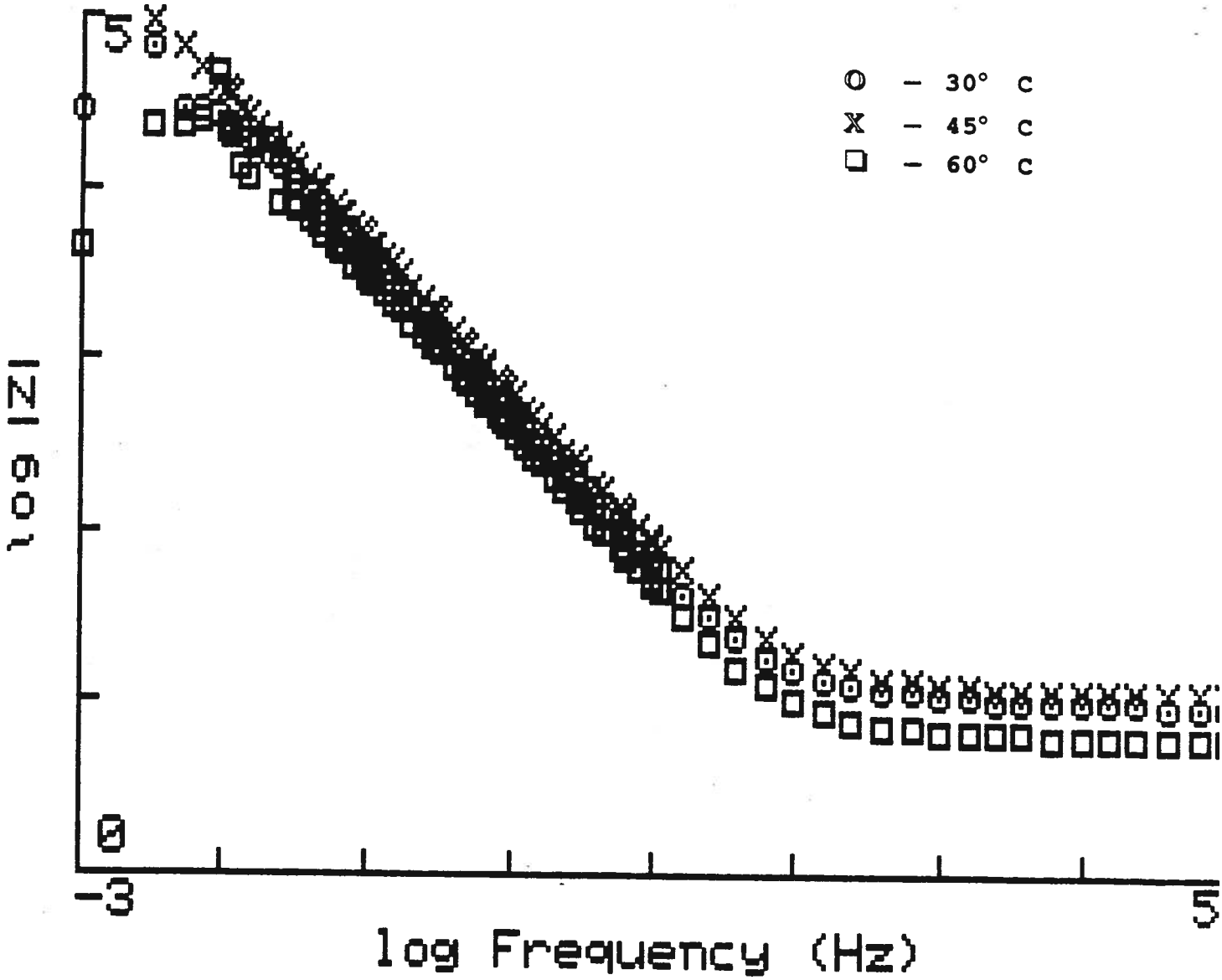

Figure 9. Initial Bode plot of |Z| vs. the log frequency for A537 carbon steel at 30°, 45°, and 60° C.

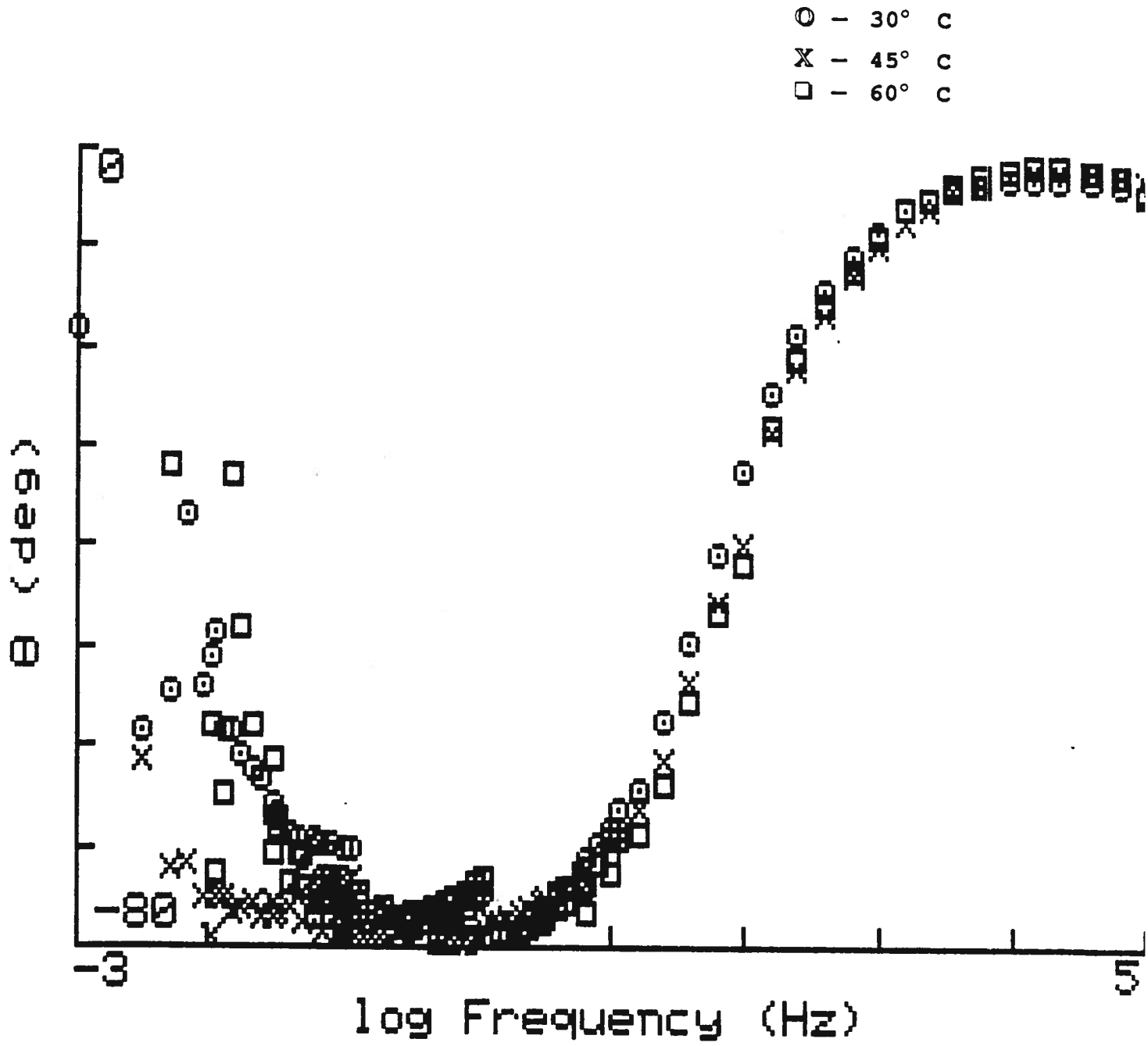

Figure 10. Initial Bode plot of the phase angle vs. the log frequency for A537 carbon steel at 30°, 45°, and 60° C.

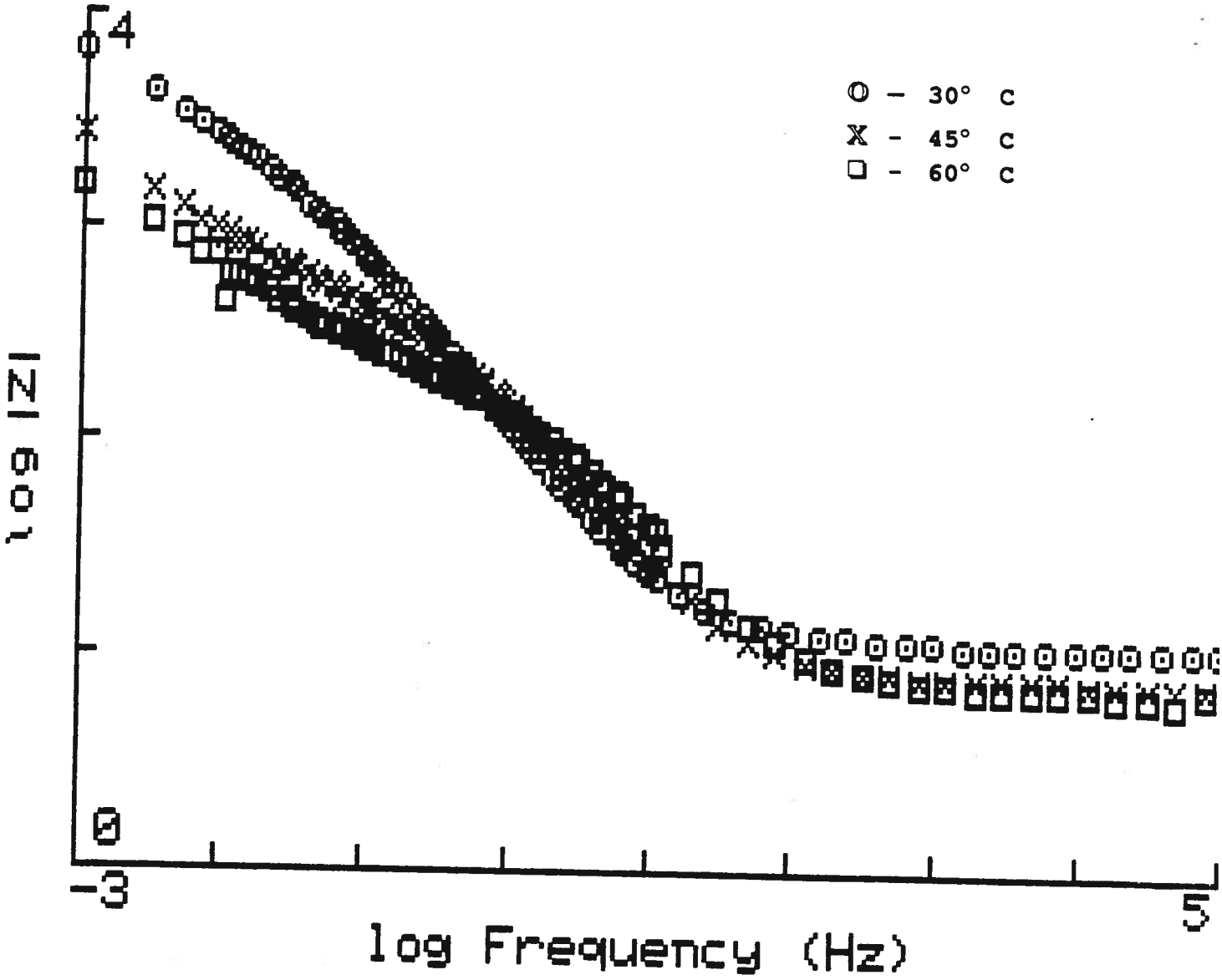

Figure 11. Final Bode plot of |Z| vs. the log frequency for A537 carbon steel at 30°, 45°, and 60° C.

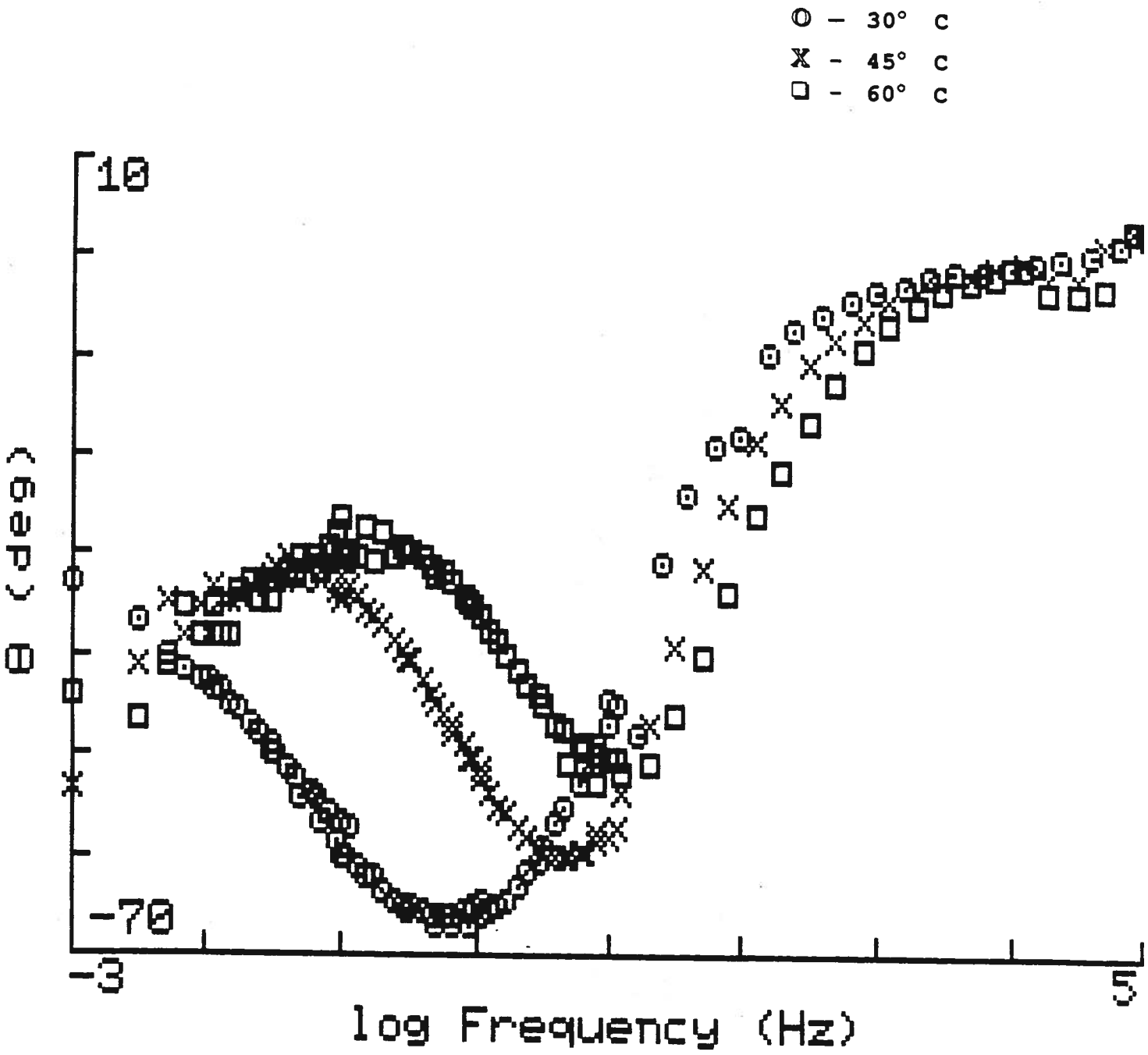

Figure 12. Final Bode plot of the phase angle vs. the log frequency for A537 carbon steel at 30°, 45°, and 60° C.

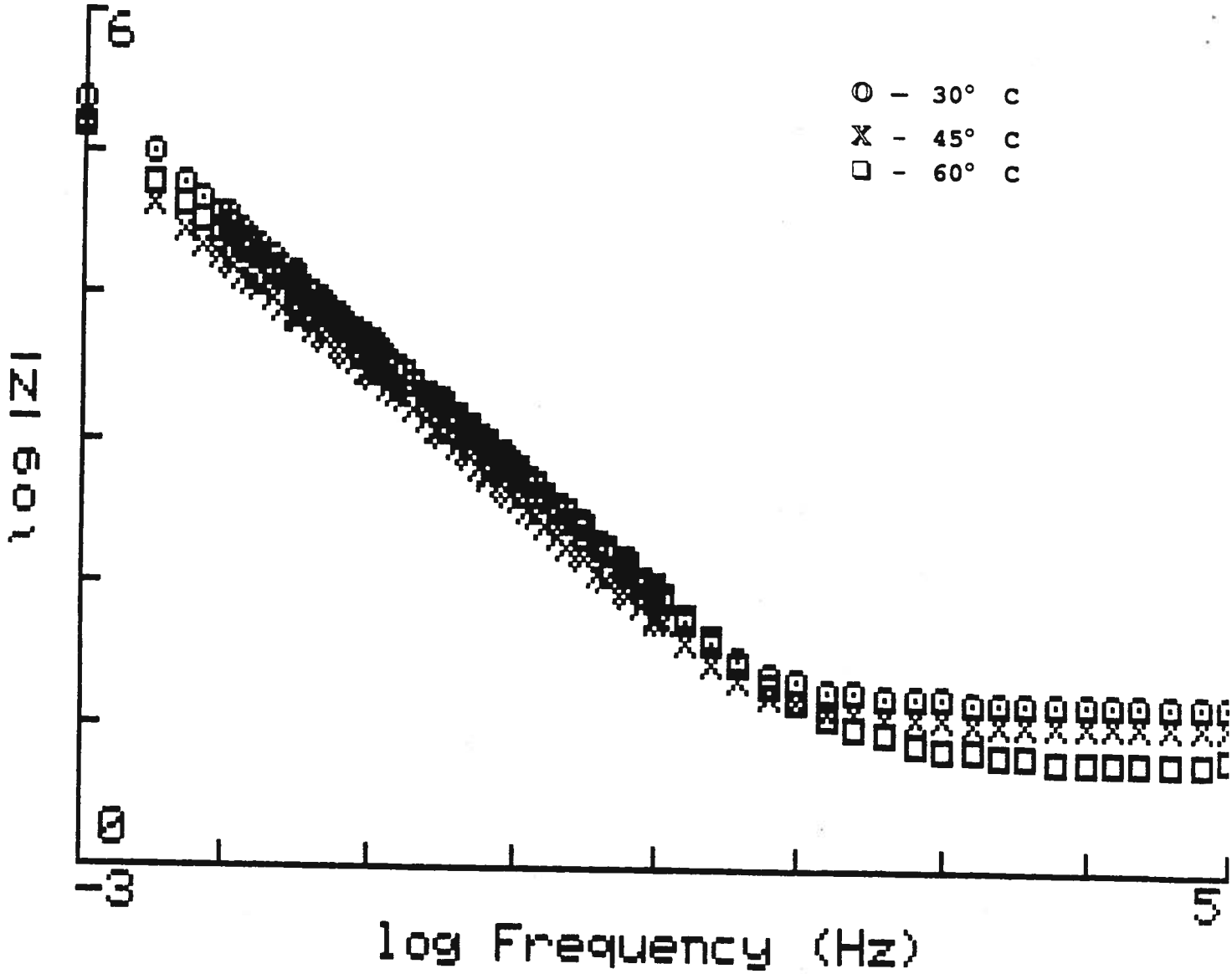

Figure 13. Final Bode plot of |Z| vs. the log frequency for 304L at 30°, 45°, and 60° C.

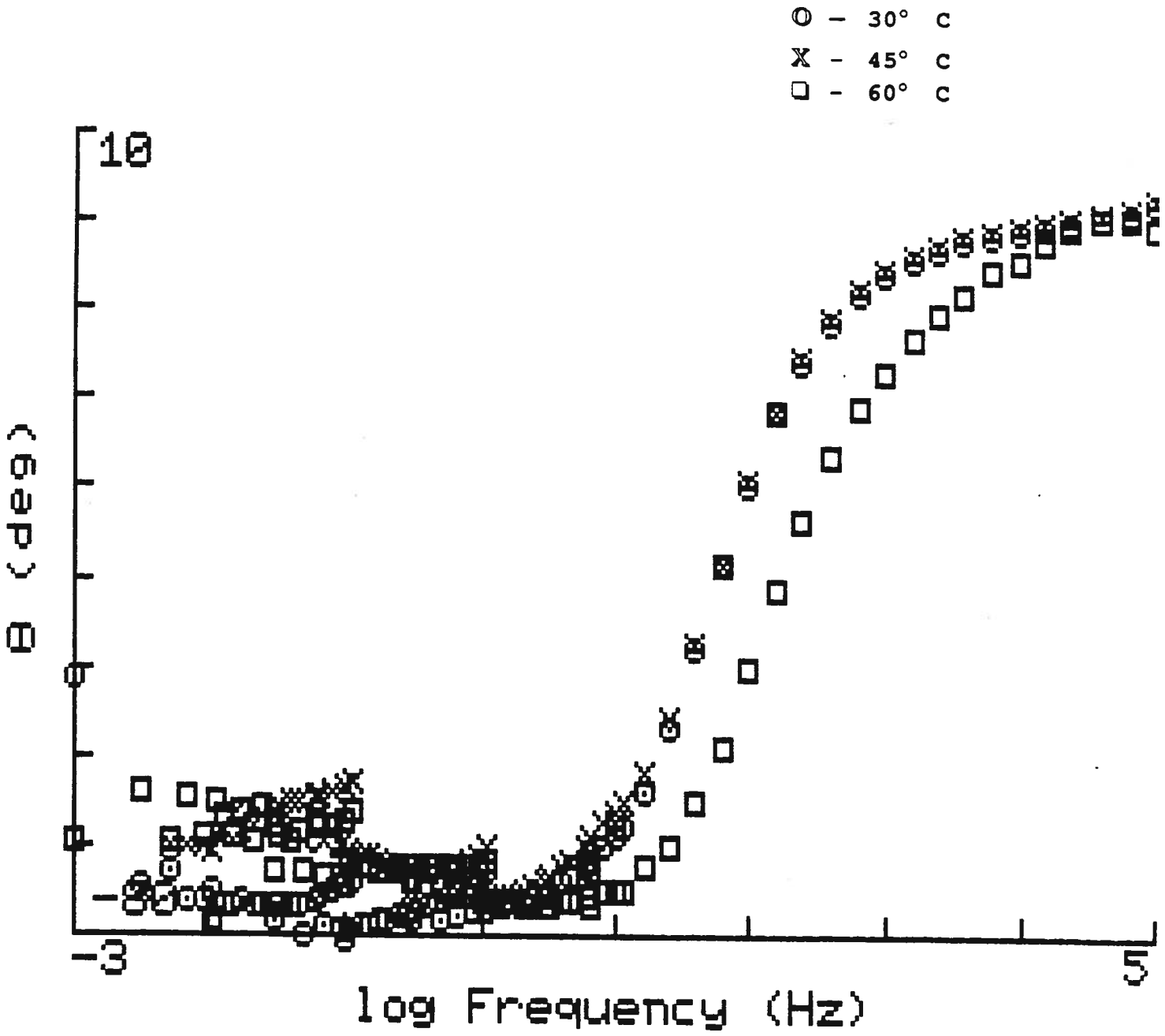

Figure 14. Final Bode plot of the phase angle vs. the log frequency for 304L at 30°, 45°, and 60° C.

This Page Intentionally Left Blank